POLITECNICO
MILANO 1863

SCUOLA DI INGEGNERIA INDUSTRIALE
E DELL'INFORMAZIONE

Executive Summary of the Thesis

Thermo-mechanical properties and microstructural evolution of thin films for nuclear applications

Laurea Magistrale in Nuclear Engineering - Ingegneria Nucleare

Author: Luca Castronuovo

Advisor: Prof. Marco Beghi

Academic year: 2022-2023

1. Introduction

In recent decades, the significance of thin films has grown considerably, playing a pivotal role in enhancing substrate properties like corrosion and wear resistance. These films also contribute to the modification of optical, electrical, or magnetic characteristics. Notably, they are extensively employed in the energy sector for developing advanced batteries and photovoltaic panels. The exploration of thin films extends to studies on materials for fusion reactors, such as the ITER project and TOKAMAK reactor, as well as fourth-generation fission reactors, particularly LFR lead-cooled reactors. Thin films are being considered as a potential solution to address significant technological challenges posed by aggressive environments in these reactors. In the case of TOKAMAK-type reactors, where extreme thermal loads, high neutron fluence, and the presence of energetic plasma particles are prevalent, the choice of an inert material becomes crucial. This material must undergo minimal changes in microstructural characteristics and mechanical properties to resist instabilities resulting in thermal loads reaching GWm^{-2} and temperatures exceeding 1000°C. Simultaneously, the material should maintain robust mechanical properties without failure. Researchers are investigating coatings of ceramic materials like alumina (Al_2O_3) or alumina with yttria Y_2O_3 deposited through the PLD (pulsed laser deposition) technique. These coatings have demonstrated resistance to the LME phenomenon, safeguarding the substrate from corrosion and ensuring resilience against typical reactor phenomena induced by radiation, such as swelling, embrittlement, and recrystallization. Furthermore, when deposited in an amorphous or ultra-nano-crystalline form, these coatings exhibit metallic characteristics, such as increased ductility [4][5]. Additionally, proposals include the use of metallic coatings like Al and Fe-Al for internal structures, steam generators, DHR heat exchangers, and primary pumps on AISI 316LN substrates [1]. It is necessary, therefore, to investigate the thermomechanical properties of thin films, such as stiffness, tenacity, mechanical strength, and thermal expansion by keeping in mind that:

- thin films do not have the same properties as the bulk material, as the reduced thickness and average crystalline grain size, as well as the presence of the substrate, (which, due to the constriction at the interface, changes the ability of the film to deform), modify the atomic bonds and

the deformation mechanisms. Generally, nanocrystalline thin films result in a higher strength and a lower stiffness than bulk material[9][8].

- measuring film properties cannot be done with the traditional techniques adopted for bulk materials, i.e., imposing a stress state and recording the material response, because of the small size of the film and the presence of the substrate.

The microstructural and mechanical properties of the films depend strongly on the deposition techniques and the parameters adopted in them. It is of interest to understand how microstructure influences thermo-mechanical properties in order to be able, even qualitatively, to predict the behavior of a film. In particular, predicting the coefficient of linear thermal expansion allows us to determine the magnitude of the stresses that develop in the film as a result of the application of a thermal load or repeated thermal cycles, evaluating the resistance of the film-plus-substrate system to thermal fatigue. In addition, the study of the stiffness and mechanical strength of the films gives us an indication of how resistant they are to wear, this being well described by the ratio H/E, with H hardness and E Young's modulus.

2. Thermo-mechanical characterization

Techniques used are **Brillouin spectroscopy** for the investigation of the elastic properties of the film and the **Wafer Curvature Technique** for the analysis of the residual stresses and CTE.

2.1. Brillouin spectroscopy

Brillouin spectroscopy is based on the interaction of laser light (λ=532nm) with the acoustic phonons of the material under investigation. For metallic materials, opaque for this wavelength, the interaction occurs at the surface thanks to the surface acoustic waves (SAWs). The can be seen as a ripple on the surface that, creating a diffraction grid, allows the interaction with the light. The scattered light can acquire or loose an amount of energy equal to the quantum of vibratial energy (phonon) relative to that particular mode.

Looking at (**Fig. 2**), the energy conservation implies that:

$$|\boldsymbol{k_s}| - |\boldsymbol{k_i}| = \pm|\boldsymbol{q}| \quad (1)$$

Variation in light frequency (thus, in energy), gives us information about the velocity of the surface acoustic modes, that are strictly related to the material's elastic constants. Involving the surface, only the component of the light-wave wavevector parallel to the surface interacts. Thus, measuring frequency shifts at different incident angles gives us a dispersion relation.

SAWs intensity decreases exponentially with depth, with a decay constant similar to the wavelength; so, if the film thickness is lower than the inspected wavelength, the interaction of the substrate becomes really important(Fig.2).

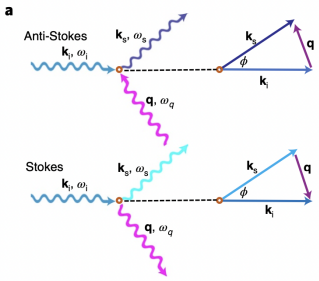

Figure 1: Interaction and momentum conservation in the laser light-phonon interaction. Figure from [6]

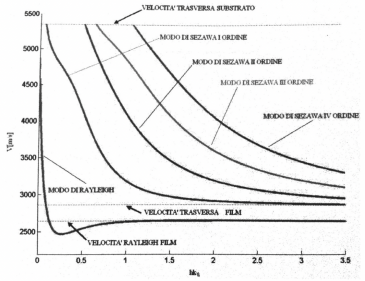

Figure 2: Dispersion relation of a W thin film on a Si substrate. In absissa, the product of the surface wavenumber $k_{//}$ and film thickness h; in ordinates, the velocities associated to Rayleigh and Sezawa modes. Figure from [2]

2.2. Wafer curvature technique

It thin film and substrates have different CTEs, the substrate will curve under a temperature gradient. If the elastic properties are isotropic,

the film thickness is constant and the adhesion is perfect, the substrate will assume the form of a spherical cap. Analogously, the residual stresses due to growth mechanisms or lattice mismatch will produce the same shape. The substrate curvature κ and the stress in the film σ_f are linked by film and substrate thicknesses t_f and t_s, and the substrate elastic properties (E_s,ν_s) through the Stoney relation:

$$\kappa = \frac{1-\nu_s}{E_s}\frac{6\sigma_f t_f}{t_s^2} \tag{2}$$

Consequently, upon measuring the substrate curvature, the stress within the film can be determined. Given that the curvature resulting from temperature variations is typically very slight, with a curvature radius on the order of 100 m, an exceptionally precise method should be employed. This method involves the deflection of parallel laser beams. In the presence of curvature on the sample, the incident parallel beams reflect in a diverging or converging manner. The change in the position of the beams is then recorded by a sensor positioned at a certain distance from the sample, obtaining a stress vs temperature plot, that gives us information about the elastic and plastic behaviour of the film. Moreover, knowing also the elastic properties of the film, we can determine the CTE.

3. Experimental Setup

3.1. Brillouin spectroscopy

The experimental setup used for Brillouin spectrospcopy includes a laser, optical systems and collection lenses, a Fabry-Perot interferometer, a photomultiplier tube and a chain of electroning components, devoted to signal's processing and elaboration. Because the great majority of photon's emission belongs to elastic peak and inelastic scattering cross-section is very small, a high revelation efficiency is required. Thus, a tandem **multi-pass Fabry-Perot interferometer** is used to resolve the low frequency shift of Rayleigh surface waves (some GHz). The **backscattering** configuration is used. Once obtained the spectra for each sample at different angles, velocities of one or more modes are registered for each wavenumber. Then, using Christoffel equations, with the right boundary conditions, we obtain the theoretical velocities for given elastic constants C_{11}, C_{44} (assuming an isotropic material). Performing a sum of the squared difference between the theoretical values and the measured ones on all angles and modes, we obtain a map with the level curves of the mean square estimator in the (C_{11},C_{44}). Then, individuated a confidence region, we are able to give the elastic constants values of the film and their uncertainties.

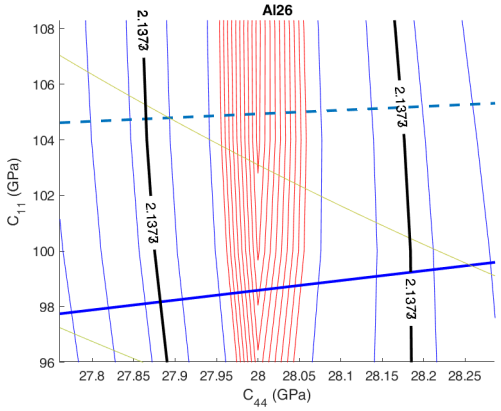

Figure 3: LS level curves. Red curves represent lower values of LS. The straight continue line represent the bulk modulus (K_{bulk}) of bulk material, while the dotted one the ratio (G/K_{bulk}), set as bounds for C_{11}. Black curve represents the 68% confidence region

3.2. Wafer curvature technique

The WCT apparatus consists of laser optics, a vacuum chamber, and a CMOS sensor used to measure the position of the laser beam, recorded as spots. The sample is posed in a vacuum chamber ($P<10^{-5}$mbar) and heated, through an alumina plate and a power supply (184 W). The laser beams consist of a 2×2 array, spaced evenly at 1 cm intervals.The array strikes the sample surface at a 60° angle of incidence at its center, and the measurement position remains constant throughout the entire measurement process. The reflected beams are captured by the CMOS camera with the aid of a collecting lens. A thermocouple, positioned under the sample, is linked to a Data Acquisition system (DAQ device), enabling a seamless and automated cycle of temperature measurements carried out using a LabVIEW Virtual Interface. A MATLAB® code for spots centroids' determination and their distances as a function of temperature has been used.

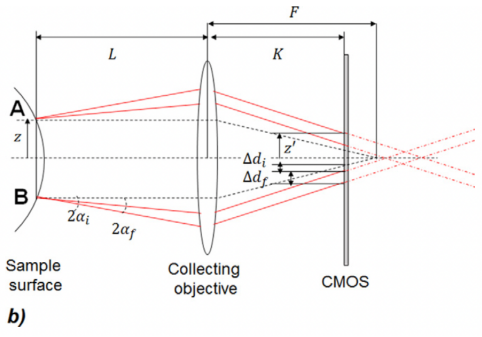

Figure 4: (a)Parallel beams deflection on a curved sample, (b)optical path from the "rays" POV [3]

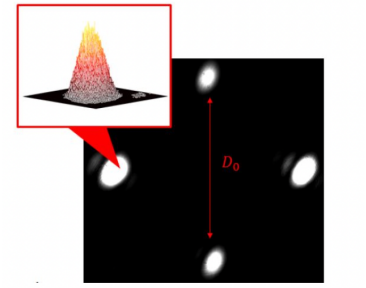

Figure 5: Spots on the sensor; Intensity profile can be seen.[7]

4. Results and Discussion

At first, samples have been elastically-characterized through Brillouin spectroscopy. Through Wafer Curvature, residual stresses has been assessed, as well as CTE, stress-relaxation's behaviour and plastic flow. Several thermal cycles have been performed on each samples to increase the accuracy of the resuslts. SEM images have been acquired before the measurements, and, in some cases, after.

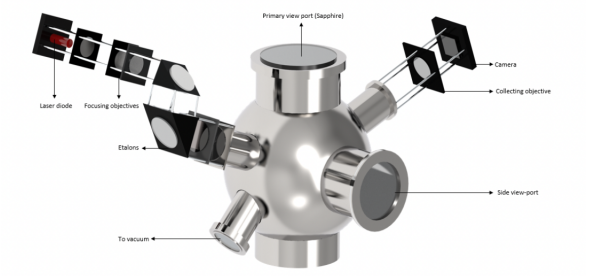

Figure 6: Vacuum chamber and optical system[7]

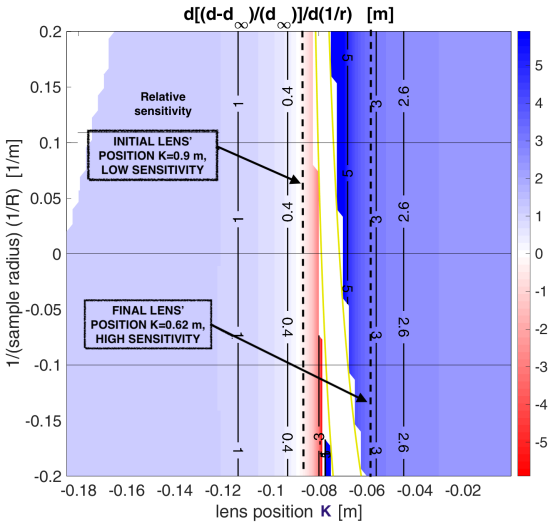

Figure 7: Relative sensitivity $\frac{1}{d_\infty}\frac{d(\Delta d)}{d(1/R)}$

4.1. Samples

Micro-, nano- and ultra-nano-crystalline samples deposited with HiPIMS and PLD at NanoLab@Polimi have been characterized. In particular, Al and W thin films (DC, HiPIMS and PLD), WN thin films (HiPIMS) and Y_2O_3 thin film (PLD).
Different samples exhibiting varied microstructures and densities were produced using a substrate bias in HiPIMS and a background gas (He) in PLD.

4.2. System Optimization

Regarding the optimization of the system, enhancements were made to the WCT's optical system to heighten sensitivity. Analysis revealed that the accuracy of system curvature measurement heavily relies on the positioning of the lens (Fig.4). By adjusting the lens position, sensitivity was amplified by a factor of 6 (Fig.7). Additionally, the series connection of heating modules allowed for a peak temperature of 650°C, a substantial increase of about 300°C compared to the maximum temperature achieved in prior work[7]. Several minor adjustments were implemented within the framework, including improvements in beam focusing, electrical insulation, and optimization of analysis software. Finally, a pyrometer was employed to evaluate temperature homogeneity, showcasing a maximum temperature deviation of less than 1%.

4.3. Brillouin results

Brillouin results confirmed a good correlation between material crystallinity, Young Modulus and other elastic properties. As said, lower-density nanocrystalline materials are ofetn associated with a higher void fraction, hence a lower mean interatomic bond.

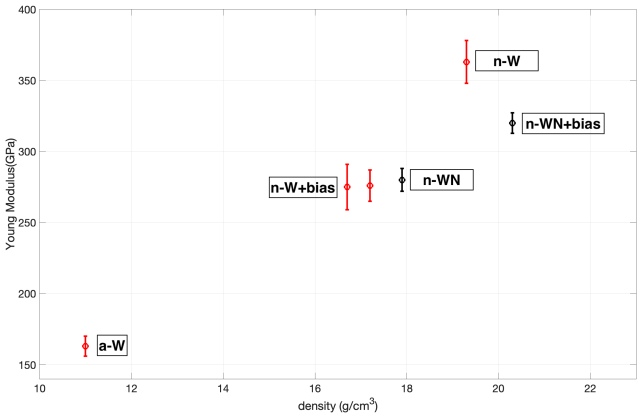

Figure 8: Young Modulus of W samples (red) and WN samples (black).

As depicted in Fig.8, there exists a correlation between the Young's modulus and both density and microstructure. HiPIMS samples from biased W exhibit reduced density attributed to heightened Ar inclusion[10]. Conversely, the biased-WN samples' lower density results from a higher nitrogen content forming chemical bonds with W, thereby augmenting its amorphous nature. The pure amorphous tungsten, deposited with PLD and He as backgraoung gas (70Pa), has a low density (11 g/cm^3), but non-porous structure shows the lowest E (163 GPa), while the highest value (365 GPa) is reached for high-density n-W.
The measured values for aluminum samples indicate that the DC sample demonstrates higher values compared to the HiPIMS samples. Additionally, the biased sample exhibits increased porosity alongside a lower Young's modulus.
Moreover, Brillouin spectra enable the evaluation not only of the shear modulus but also of the Poisson ratio.

4.4. Wafer Curvature Results

Through WCT, it was possible to determine the residual stresses present in the samples before and after heating. Large compressive stresses, up to 1 GPa, were observed in tungsten samples

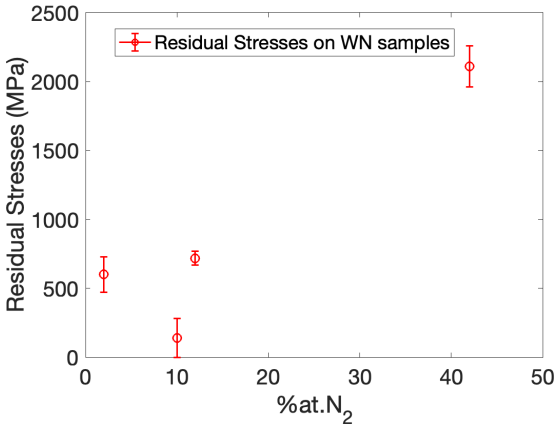

Figure 9: Measured residual stresses of the as-deposited samples

deposited with HiPIMS, slightly higher for samples to which a time delay was applied in the bias. For the WN samples,compressive stresses between 500 and 1000 MPa were measured. In the case of the sample containing 42% N, the residual stresses exceeded 2 GPa, causing buckling failure el sample. Following the measurement of residual stresses, multiple thermal cycles were executed on each sample, generating a Stress vs Temperature plot. Initially, a linear trend is observed, succeeded by a non-linear pattern attributed to stress-related phenomena like structural relaxations, densification, and localized plastic flow. These processes can induce microstructural and shape changes, such ass the formation of hillocks, resulting from a compressive stress relaxation.

4.4.1 Non-linear behaviour

The linear segment can give information about the difference in CTEs between the film (f) and the substrate (s). The slope is given by $[E_f/(1-\nu_f)]\Delta(CTE)$. Several cycles can improve the accuracy of the CTE determination. Fig.10 illustrates an initial linear trend succeeded by a non-linear shape associated with plastic deformation. This deformation showcases a densification effect, i.e., an increase in grain mean size coupled with the development of tensile stress. Hillock formation has been confirmed by a SEM planar view for an Al specimens. Pre-existing hillocks, formed by a strain-induced abnormal grain growth, increased in size thanks to compressive stress relaxation due to heating. A strain-hardening effect can be seen, as the non-

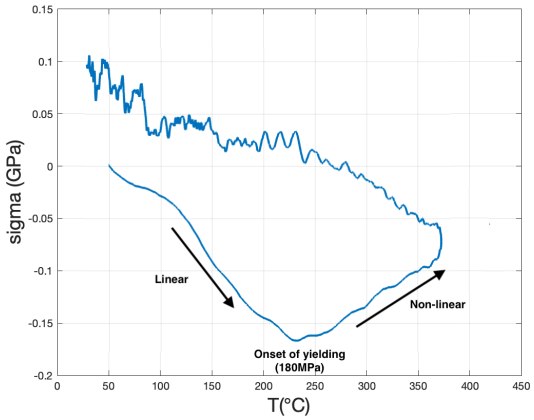

(a)

Figure 10: Stress vs Temperature: the non-linear behaviour of an Al sample is shown

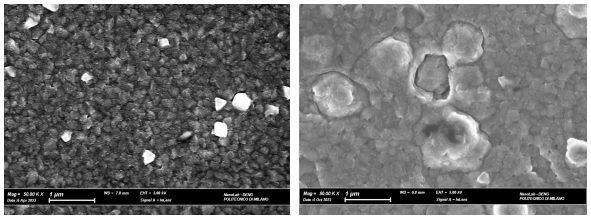

(a) (b)

Figure 11: Al-27 as deposited (a), and after heating (b). Small hillocks before heating can be seen (brighter grains), that became large after heating

linear behaviour occurred at higher compressive stresses cycle after cycle. A strong densification effect due to structural relaxation (but not grain growth) can be observed also in WN samples and in amorphous W-sample. The measurements of Coefficient of Thermal Expansion (CTE) revealed minimal disparity compared to the bulk CTE, except for the amorphous sample a-W, which displayed a notably higher value. This outcome indicates that despite the low grain dimensions that might predict higher values, the compact structure induced by HiPIMS and the substantial residual stresses limit the material's expansion. Moreover, the values for aluminum demonstrated a lower CTE compared to the bulk value.

5. Conclusions

In this study, we conducted a comprehensive characterization of the thermo-mechanical properties of thin films made of Aluminum, Tungsten, and Tungsten-Nitride. Our focus extended to establishing correlations between deposition techniques, film microstructure, and the elastic, plastic, and thermal properties of these films. To achieve this, we employed Brillouin spectroscopy and the Substrate Curvature Technique, optimizing the measurement system for heightened sensitivity and accuracy. Significant enhancements were achieved in the Substrate Curvature Technique, with a relative sensitivity increase by a factor of approximately 6. The measurements of coefficient of thermal expansion (CTE) reveal no significant difference between the HiPIMS-deposited samples and the bulk material, with a lower CTE observed for aluminum. In contrast, samples deposited using Pulsed Laser Deposition (PLD) generally exhibit a higher CTE. This disparity may be attributed to the high compactness and density structure of HiPIMS samples, which provides a high atomic bond similar to the bulk material.This observation is promising, especially when considering the thermal fatigue that a tungsten film may experience in nuclear applications, potentially minimizing thermal loads. However, it's essential to note that the high residual stresses developed with HiPIMS can lead to failure at lower temperatures. Furthermore, a higher yield strength is associated with a greater hardness (H). The ratio of hardness to Young's modulus (H/E) serves as a reliable indicator of a material's wear resistance. As crystallinity and thickness decrease, yield strength increases, and Young's modulus decreases. This leads to an improved wear resistance, making these films well-suited for Generation IV nuclear applications.

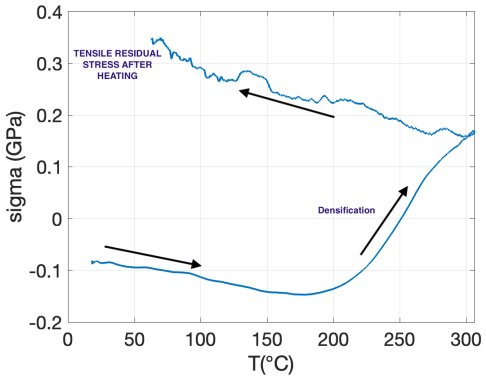

Figure 12: Stress Temperature Diagram for a-W

However, the microstructure instability of Al thin films can lead to the formation of hillocks

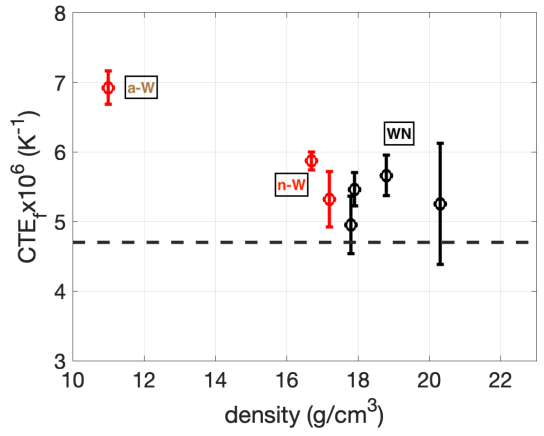

(a)

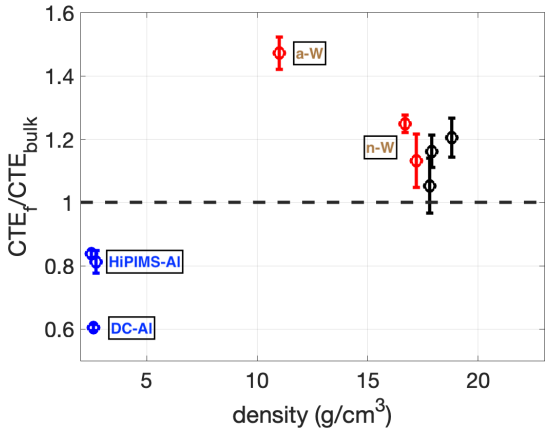

(b)

Figure 13: (a)CTE values of W samples, the dotted line represent the value of bulk-W CTE. (b)Ratio between CTE_{film} and CTE_{bulk} for W(red), WN(black) and Al(blue)

and abnormal grain growth, and prevents it for being used at very high temperatures.

6. Acknowledgements

We express our gratitude to Marco Beghi for his invaluable assistance and constructive feedback. Additionally, our thanks extend to Luigi Bana and Davide Vavassori for generously providing the samples. Their contributions have been instrumental in our work.

References

[1] Overview on lead-cooled fast reactor design and related technologies development in enea. *Energies*, 14:5157, 08 2021.

[2] E. Besozzi. Caratterizzazione di film di tungsteno mediante spettroscopia brillouin. Master's thesis, Politecnico di Milano, Corso di Laurea Magistrale in Ingegneria Nucleare, 2012.

[3] E. Besozzi, D. Dellasega, A. Pezzoli, A. Mantegazza, M. Passoni, and M.G. Beghi. Coefficient of thermal expansion of nanostructured tungsten based coatings assessed by substrate curvature method. *Materials & Design*, 137:192–203, 2018.

[4] Francisco García Ferré, Emanuele Bertarelli, Angelica Chiodoni, Davide Carnelli, Dario Gastaldi, Pasquale Vena, Marco G. Beghi, and Fabio Di Fonzo. The mechanical properties of a nanocrystalline $Al_2O_3/a-Al_2O_3$ composite coating measured by nanoindentation and brillouin spectroscopy. *Acta Materialia*, 61(7):2662–2670, 2013.

[5] F. García Ferré, A. Mairov, L. Ceseracciu, Y. Serruys, P. Trocellier, C. Baumier, O. Kaïtasov, R. Brescia, D. Gastaldi, P. Vena, MG. Beghi, L. Beck, K. Sridharan, and F. Di Fonzo. Radiation endurance in Al_2O_3 nanoceramics, 2016.

[6] Fariborz Kargar and Alexander A. Balandin. Advances in brillouin–mandelstam light-scattering spectroscopy. *Nature Photonics*, 15(10):720–731, 2021.

[7] Vishakha Nagarajan. Optimization of the Experimental setup for Substrate Curvature Method. Master's thesis, Politecnico di Milano, Milan, 12 2021.

[8] William D. Nix. Mechanical properties of thin films. *Metallurgical Transactions A*, 20(11):2217–2245, 1989.

[9] Carl V. Thompson and Roland Carel. Stress and grain growth in thin films. *Journal of The Mechanics and Physics of Solids*, 44:657–673, 1996.

[10] D. Vavassori, F. Mirani, F. Gatti, D. Dellasega, and M. Passoni. Role of magnetic field and bias configuration on hipims deposition of w films. *Surface and Coatings Technology*, 458:129343, 2023.